

Multi-dimensional seismic response control of offshore platform structures with viscoelastic dampers (I-Theoretical analysis)

Xiao-Yu He^{*1}, Hong-Nan Li² and Jun Zhang³

¹Zhejiang Provincial Planning, Design & Research Institute of Communications, Hangzhou 310006, P.R. China

²State Key Laboratory of Coastal and Offshore Engineering, Dalian University of Technology, Ganjingzi District, Linggong Road 2, Dalian, 116024, P.R. China

³State Grid Zhejiang Electric Power Company, Hangzhou, 310007, P.R. China

(Received December 31, 2015, Revised April 6, 2016, Accepted April 7, 2016)

Abstract. Based on classical viscoelastic damper, a brand-new damper is designed by the change of simple construction to implement vibration control for both translational vibration and rotational vibration simultaneously. Theoretic analysis has been carried out on the restoring force model and the control parameters. Two improved models are presented to obtain high simulation precision. The influence of the size, shape of the viscoelastic material, the ambient temperature and the response frequency on the vibration control effect is analyzed. The numerical results show that the new type viscoelastic damper is capable of mitigating the multi-dimensional seismic response of offshore platform and the response control effect has complicated relations with aforementioned related factors.

Keywords: viscoelastic damper; platform; multi-dimensional seismic response; seismic control

1. Introduction

During the past few years, extensive analytical and experimental investigations have been carried out to investigate the performance of viscoelastic dampers (VED) as energy-dissipation devices for structural applications (Mahmoodi 1969, Lin, Liang *et al.* 1991, Chang *et al.* 1992, Bergman and Hanson 1993, Chang *et al.* 1995). Results from these studies showed that the response of structures to earthquakes can be reduced significantly due to notable increase in measured structural damping. The corresponding structural responses due to seismic loading also decreased accordingly. However, analytical and test results also showed that, although the damper can be effective in attenuating seismic response of the structure, the proper design for maximum efficiency must take into account important factors such as excitation frequency, structure natural frequency and working environment temperature.

A typical VED consists of thin layers of viscoelastic material and steel plates. So far researchers all over the world have developed multiform VEDs (Zhou 2006), such as bitumen rubber composition (BRC) VED, lath-type VED, arm-type VED, lever VED, distinguished

*Corresponding author, Ph.D., E-mail: rainy0649@126.com

themselves on constitution and viscoelastic material from the typical VED. Viscoelastic Damper is also one of the most popular control devices for the seismic control research of offshore platforms. Lee(1997) used VED to mitigate the vibration of an offshore structural system in the marine environment and verified that the VED has high energy absorption capacity. Ou *et al.* (Ou *et al.* 1999, Ou *et al.* 2000, Ou *et al.* 2002) analyzed the dynamic performances of the platform structure with a set of viscoelastic energy dissipators. Ma *et al.* (Ma *et al.* 2004) studied the dynamic response of an actual multi-degree freedom offshore platform equipped with viscoelastic dampers and optimized the position of VED. The VED absorbs earthquake energy by transforming the shear deformation energy into heat. However, typical VEDs are usually installed in single frame side of structures connected by braces and work only in one horizontal direction. However, the new-type VED developed in this paper will be proposed due to its superiority of capacity for bi-directional shear deformation. It is known that earthquake motion is essentially multi-dimensional and so is the corresponding structural response. Therefore, multi-component seismic response of offshore platform can be controlled by installing typical VEDs in both frame side directions and can also be well controlled by installing the proposed new-type VED in single deck plane.

When using VEDs, effective modeling of the frequency- and temperature-dependent characteristics of the VED plays a key role in accurate simulation of structural responses analysis. Models for the constitutive behavior of viscoelastic material have been proposed by a number of researchers using fractional derivatives and equivalent standard solid techniques (Kasai *et al.* 1993, Xu *et al.* 2001). These two models can also capture the temperature-dependence of the properties of the VED using the so-called "Temperature-frequency equivalence principle". However, these two models do not necessarily capture the actual behavior of the VED over the ambient temperature range for practical engineering. Further study on their modeling precision is still needed to carry on.

This paper is concerned with the multi-dimensional seismic control behavior of a viscoelastically damped structure under earthquake ground motions. A brand-new damper is designed by the change of simple construction to implement vibration control for both translational vibration and rotational vibration simultaneously. Then two improved models are presented to obtain high simulation precision for theoretic analysis. In the end, the influence of the size, shape of the viscoelastic material, the ambient temperature and the response frequency on the vibration control effect is analyzed.

2. Working principle for the multi-dimensional control of viscoelastic dampers

The new-type VED used in this paper is different from the typical VED in both construction feature and installation form. Schematic diagrams for the construction and installation form are shown in Figs. 1 and 2 respectively. The essential difference between the two types of VEDs lies in the plane relationship between viscoelastic material and platform deck. When the deformation of platform deck occurs in all possible directions, bi-directional shear deformation will take place in the new-type VED with parallel position relationship between viscoelastic material and platform deck while unidirectional shear deformation will take place in the typical VED with perpendicular position relationship between viscoelastic material and platform deck. Due to its bi-directional deformation capacity, the new-type VED can consume more energy than the typical VED. Hence the cost of seismic control can be reduced.

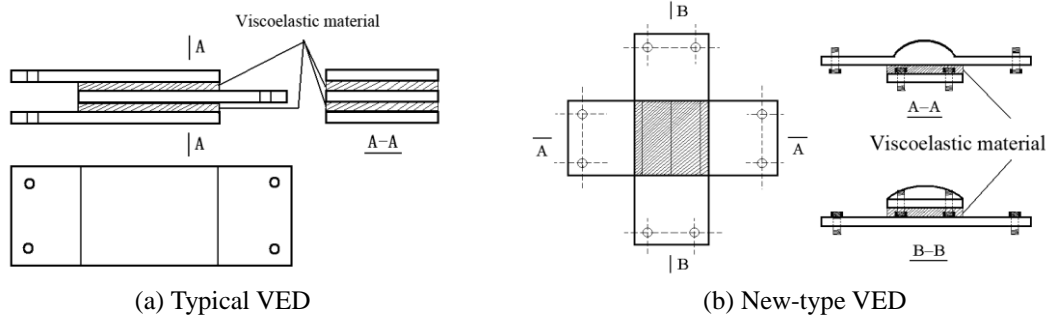


Fig. 1 Structure scheme for the viscoelastic dampers

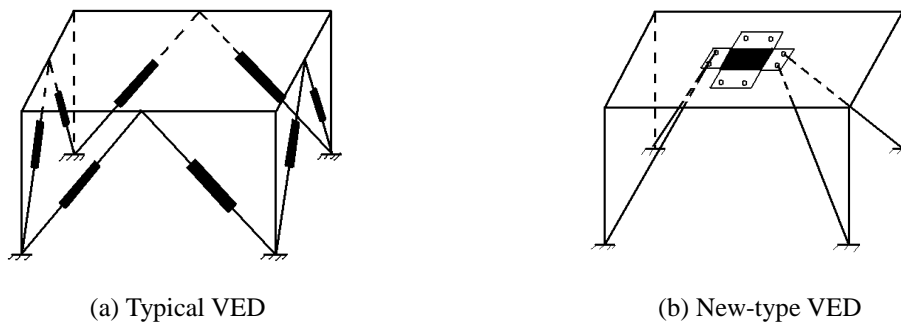


Fig. 2 The Setting of different viscoelastic dampers

3. Improved restoring force model

Many studies and tests on VEDs have shown that the energy absorption properties are dependent on the ambient temperature, excitation frequency and strain amplitude. Several mathematical models, such as the Kelvin model, Maxwell model, standard linear model, complex parameter model, four parameters model, equivalent standard solid model and fractional derivative model have been proposed for reproducing the experimental behavior of VEDs. Of these, only the equivalent standard solid model and the fractional derivative model can reflect the influence of temperature and frequency on VEDs.

3.1 Equivalent standard solid model

Temperature and frequency are the main factors that affect the energy dissipation property of VEDs. Previous research (Chang *et al.* 1992, Inaudi 1996) has shown that the storage modulus G' (which reflects the VED's stiffness) decreases with increasing temperature and increases with increasing frequency, and the loss factor η (which reflects the VED's energy dissipation capacity) has an optimum value which varies with temperature and frequency. The Kelvin model, Maxwell model and standard linear solid model are usually used to simulate VED's energy dissipation property. The Kelvin model of VED consists of a linear spring in parallel with a viscous element,

and the Maxwell model consists of a linear spring in series with a viscous element. Details of the two models are explained in the literature (Xu 2001), and thus they are not discussed in detail here.

3.1.1 The standard linear solid model

The standard linear solid model of VED consists of a linear spring in series with the Kelvin model, as shown in Fig. 3. The relationship between the stress and the strain is given by

$$\tau + p_1 \dot{\tau} = q_0 \gamma + q_1 \dot{\gamma} \quad (1)$$

where q_0 , q_1 and p_1 are coefficients related to the viscoelastic material, and τ and γ are the shear stress and shear strain, respectively. For harmonic deformation, if the Fourier transformation is applied to Eq. (1), the following equations can be obtained

$$\left. \begin{aligned} G' &= (q_0 + p_1 q_1 \omega^2) / (1 + p_1^2 \omega^2) \\ G'' &= (q_1 - p_1 q_0) \omega / (1 + p_1^2 \omega^2) \\ \eta &= (q_1 - p_1 q_0) \omega / (q_0 + p_1 q_1 \omega^2) \end{aligned} \right\} \quad (2)$$

where ω is frequency. When the frequency ω increases, the storage modulus G' and G'' can be increased by adjusting coefficients q_0 , q_1 and p_1 . It can be seen from Eq. (2) that the loss factor η will reach a maximum value at a fixed frequency. These characteristics reflect the influence of frequency on the behavior of VED, but this model cannot account for the effects of temperature on the behavior of VED.

3.1.2 Temperature-frequency equivalence theory

The storage modulus G' and the loss factor η are functions of the temperature T and the frequency ω . Studies (Xu 2007) show that the temperature effect is similar to the effects of frequency, provided that the ambient temperature of the VED is between their glass temperature. The effects of temperature and frequency on VED can be considered together if the storage modulus G' and the loss factor η are expressed as

$$\left. \begin{aligned} G'(\omega, T) &= G'(\alpha_T \omega, T_0) \\ \eta(\omega, T) &= \eta(\alpha_T \omega, T_0) \\ \log \alpha_T &= -\alpha_1 (T - T_0) / [\alpha_2 + (T - T_0)] \end{aligned} \right\} \quad (3)$$

where T_0 is the reference temperature, α_T is the temperature transformation coefficient and α_1 , α_2 are coefficients related to material property.

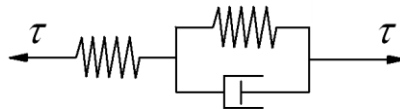


Fig. 3 Standard linear solid model

3.1.3 The equivalent standard solid model

In order to reflect the effects of temperature and frequency on VED, the temperature-frequency equivalence theory is applied to the standard linear solid model, and the equivalent standard solid model is thus created. The frequency ω in Eq. (2) will be changed into the transformed frequency $\alpha_T \omega$ and the index of frequency will be altered so as to describe the effects of both the frequency and the temperature on the parameters of the VED. The storage modulus G' and the loss factor η can be written as

$$\left. \begin{aligned} G' &= (q_0 + p_1 q_1 \alpha_T^c \omega^c) / (1 + p_1^2 \alpha_T^c \omega^c) \\ \eta &= (q_1 - p_1 q_0) \alpha_T^d \omega^d / (q_0 + p_1 q_1 \alpha_T^{2d} \omega^{2d}) \end{aligned} \right\} \quad (4)$$

where q_0 , q_1 , p_1 , c and d are parameters related to the properties of the VED, which should be determined by statistical methods from the experimental data.

3.2 Fractional derivative model

Another model that has been successfully used to capture the frequency-temperature dependence over a wide range of excitation frequencies is the fractional derivative model proposed by Kasai (Kasai *et al.* 1993). The relationship between the stress and the strain is given by

$$\tau(t) + aD^\delta \tau(t) = G[\gamma(t) + bD^\delta \gamma(t)] \quad (5)$$

Where a and b are constant, G is elastic parameter, $D^\delta = d^\delta / dt^\delta$ denotes the fractional derivative operator, and $\tau(t)$ and $\gamma(t)$ are the shear stress and shear strain, respectively.

Under cyclic loading, the storage modulus G' and the loss factor η can be written as

$$\left. \begin{aligned} G'(\omega) &= G \frac{[1 + b\omega^\delta \cos(\delta\pi/2)][1 + a\omega^\delta \cos(\delta\pi/2)] + [ab\omega^{2\delta} \sin^2(\delta\pi/2)]}{[1 + a\omega^\delta \cos(\delta\pi/2)]^2 + [a\omega^\delta \sin(\delta\pi/2)]^2} \\ \eta(\omega) &= \frac{(-a + b)\omega^\delta \sin(\delta\pi/2)}{1 + (a + b)\omega^\delta \cos(\delta\pi/2) + ab\omega^{2\delta}} \end{aligned} \right\} \quad (6)$$

In order to reflect the effects of temperature and frequency on VED, the temperature-frequency equivalence theory is also applied to the fractional derivative model. Therefore, the effects of temperature and frequency on VED can be considered together and the storage modulus G' and the loss factor η are expressed as

$$\left. \begin{aligned} G'(\omega, T_{ref}) &= G'(c\omega, T) \\ \eta(\omega, T_{ref}) &= \eta(c\omega, T) \end{aligned} \right\} \quad (7)$$

where c is the temperature-frequency transformation coefficient with its expression as

$$c = (T/T_{ref})^p \quad (8)$$

The expressions of a and b in Eq. (6) are as follows

$$a = a_{ref} / (T/T_{ref})^{\delta p} \quad (9)$$

$$b = b_{ref} / (T/T_{ref})^{\delta p} \quad (10)$$

where a_{ref} , b_{ref} are values of the parameter a and b at reference temperature T_{ref} , p is a constant related to VED. Researchers (Wu and Guo 1998) present the specific steps to determine all the parameters (a , b , δ , G and p) through experimental method.

3.3 Improved models

The equivalent standard solid model and the fractional derivative model utilize the temperature-frequency equivalence theory to realize the transformation of the storage modulus G' and the loss factor η from any temperature to reference temperature. Although the above two models adopt different definitions for the temperature-frequency transformation coefficient to describe the temperature dependence property, these coefficients (α_T and c) are so difficult to determine in the simulation of actual experiment data and are so dependent on the reference temperature assumed. The temperature and frequency ranges for VED used in civil engineering are $-30^\circ\text{C} \leq T \leq 30^\circ\text{C}$ and $0.1 \text{ Hz} \leq \omega \leq 10 \text{ Hz}$, respectively. Within these ranges, the simulation precision of the characteristic parameter G' and η using the above two models may not satisfy the demand of actual engineering project. Therefore, two improved models are presented to obtain high simulation precision for theoretic analysis based on the equivalent standard solid model and the fractional derivative model. Fig. 4 gives flow chart for the determination of the improved fractional derivative model parameters. The determination of the improved equivalent standard solid model parameters is similar to that of the improved fractional derivative model, and it is not stated here.

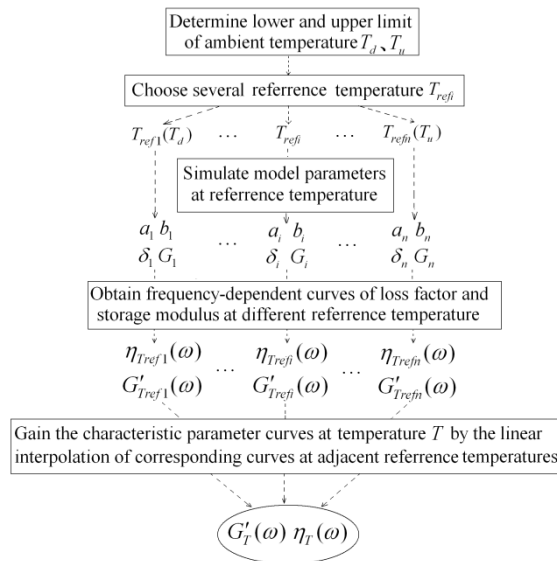


Fig. 4 Flow chart for the determination of parameters

3.4 Comparison of simulation precision for different models

Scholar Sui (2002) carried on extensive experimental researches on characteristic parameters of VED. Experimental data including the test values of storage modulus and loss factor at nine kinds of temperatures (0°C, 8°C, 12°C, 17°C, 20°C, 25°C, 30°C, 35°C, 40°C) and seven kinds of exciting frequencies (0.15 Hz, 0.3 Hz, 0.5 Hz, 1.0 Hz, 1.5 Hz, 2.5 Hz and 4.0 Hz) are used to simulate restoring force parameters by the four kinds of models: equivalent standard solid model, fractional derivative model, improved equivalent standard solid model and improved fractional derivative model (denoted as model I, II, III and IV, respectively). Genetic algorithm and direct toolbox in MATLAB program is used in this paper to calculate the model parameters. The square sum of the difference between fitting values and test values of characteristic parameters is chosen as an objective function. The calculation results of model parameters for model I are: $q_0=0.4969$, $q_1=8.3451$, $p_1=1.0165$, $c=0.8455$, $d=-0.2353$ (with the reference temperature of 20°C) and of the temperature transformation coefficients are: $\alpha_1=15.0000$, $\alpha_2=149.3929$ (calculated by test data at 17°C). The calculation results of model parameters for model II are: $G=0.7898$, $a=-0.1586$, $b=6.0840$, $\delta=0.4996$ (with the reference temperature of 20°C) and of the temperature transformation coefficient is: $p=2.7470$ (calculated by test data at 17°C). The calculation results of model parameters for model III and model IV are listed in Tables 1 and 2 respectively. Figs. 5 and 6 show the comparison of test data and fitting data of storage modulus and loss factor for the four-type models, respectively. Simulation error is defined as the ratio of the difference of fitting data and test data to test data. Tables 3 and 4 give the average simulation errors for the four types of models.

Table 1 The parameters for the improved equivalent standard solid model

$T/^\circ\text{C}$	q_0	q_1	p_1	c	d
0	-2.6010	23.3582	1.7739	0.6305	-0.2451
8	-4.8122	22.8934	1.9514	0.6013	-0.2061
12	-1.2833	15.1414	1.2106	0.4649	-0.1663
17	-0.7980	12.1961	1.2482	0.6224	-0.1777
20	0.4969	8.3451	1.0165	0.8455	-0.2353
25	0.4243	5.9676	1.0444	0.8905	-0.2577
30	0.2016	4.9129	1.2895	0.7304	-0.2943
35	0.3305	3.0613	1.1762	0.9335	-0.3766
40	0.2934	2.3670	1.1777	0.7885	-0.4056

Table 2 The parameters for the improved fractional derivative model

$T/^\circ\text{C}$	G	a	b	δ
0	0.9375	-0.5581	4.9399	0.1987
8	1.0637	-0.4775	4.3384	0.2388
12	2.0501	-0.1948	2.0230	0.3136
17	1.2537	-0.2148	3.3999	0.3812
20	0.7898	-0.1586	6.0840	0.4996
25	0.8264	-0.1089	3.9048	0.5375
30	0.8962	-0.1196	2.1485	0.5151
35	0.6194	-0.0679	2.7671	0.6371
40	0.6296	-0.0049	1.9400	0.7347

Table 3 The mean fitting errors of the storage shear modulus for the four models

Simulation error of G' (%)	0°C	8°C	12°C	17°C	20°C	25°C	30°C	35°C	40°C
Model I	22.65	16.86	8.12	3.82	2.58	14.02	29.33	29.71	34.7
Model II	NaN	90.52	16.27	9.63	5.07	14.43	21.80	59.76	78.04
Model III	0.96	0.94	1.65	2.68	2.58	3.62	3.60	6.04	7.42
Model IV	4.09	5.33	4.38	6.11	5.07	7.39	3.61	3.40	5.36

Table 4 The mean fitting errors of the loss factor for the four models

Simulation error of η (%)	0°C	8°C	12°C	17°C	20°C	25°C	30°C	35°C	40°C
Model I	166.46	86.59	28.63	9.14	1.64	16.87	22.42	33.38	43
Model II	NaN	364.79	87.77	8.81	5.32	12.01	8.73	11.46	14.6
Model III	2.95	3.91	2.03	1.50	1.64	1.30	1.96	2.75	3.68
Model IV	7.73	7.43	2.31	4.63	5.32	4.55	4.63	5.03	9.55

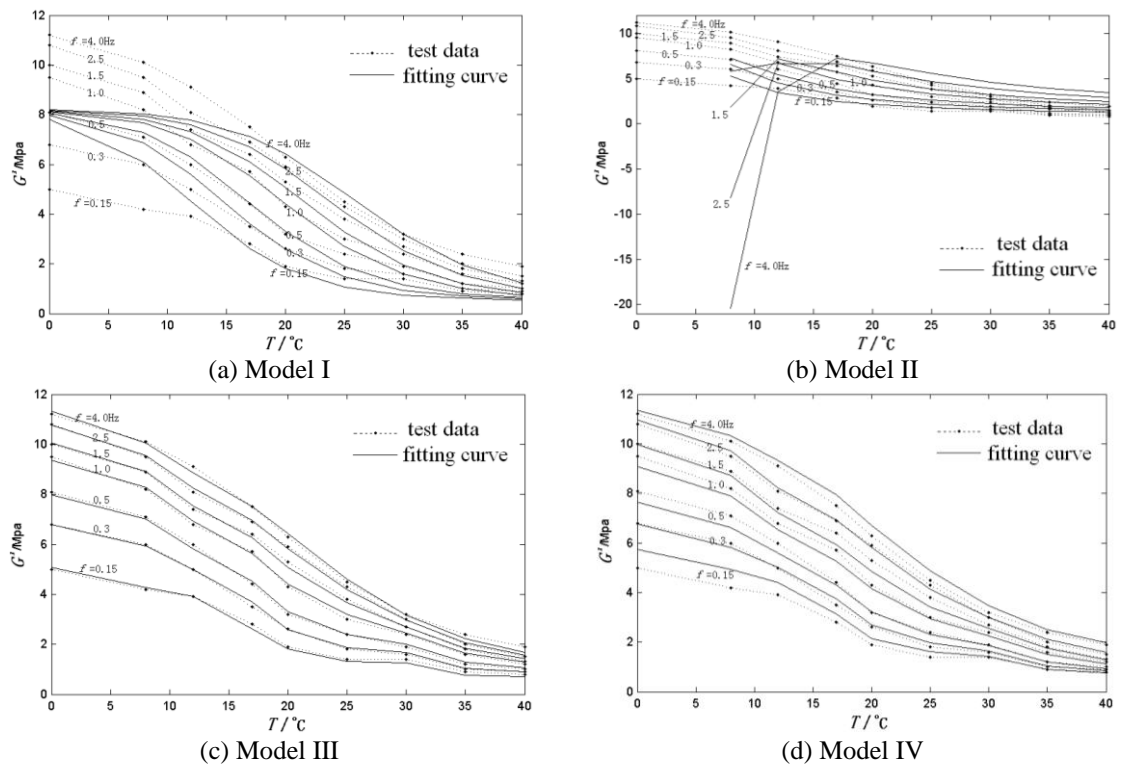


Fig. 5 The fitting curves of storage shear modulus with temperature and frequency

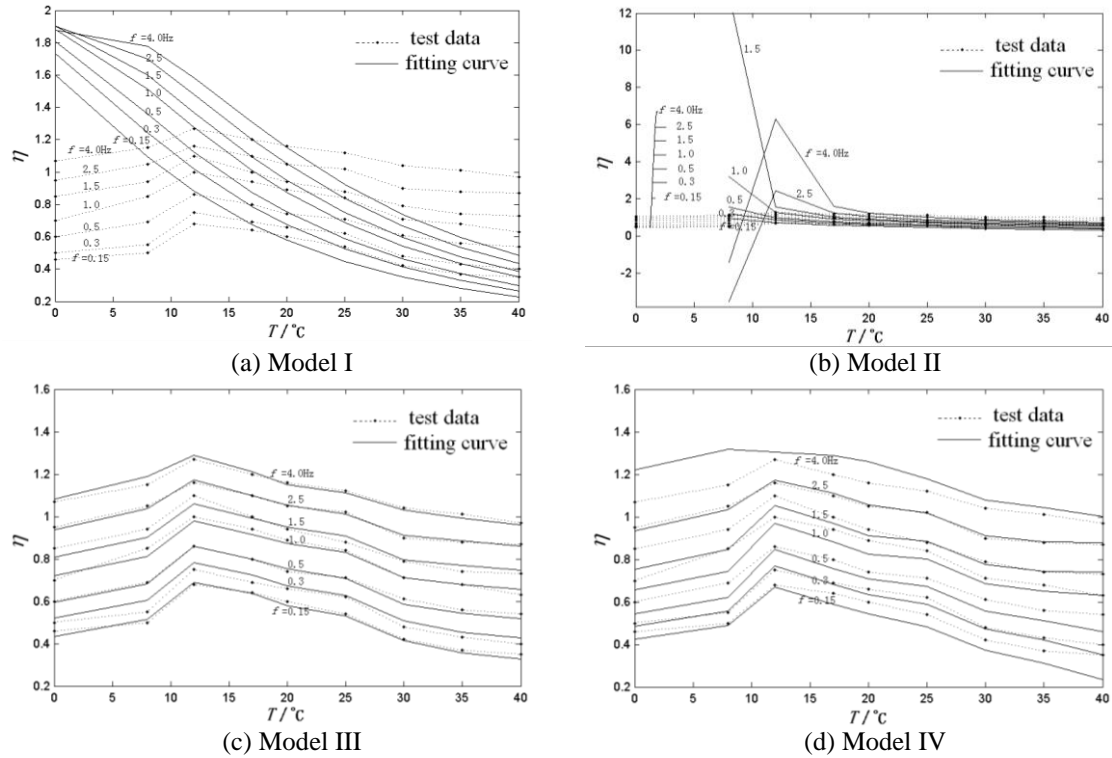


Fig. 6 The fitting curves of the loss factor with temperature and frequency

Numerical results show that the simulation precision of the frequency-dependence property of viscoelastic material is rather high at the reference temperature and will be lower with the increase of the difference $T-T_{ref}$ for model I and model II. However, the simulation precision is satisfied over a wide range of ambient temperature for model III and model IV which are presented in this paper. When $0^\circ\text{C} \leq T \leq 30^\circ\text{C}$, the simulation precision of the storage modulus with the maximum simulation error of 3.62% is higher for model III than model IV, and when $30^\circ\text{C} \leq T \leq 40^\circ\text{C}$, that simulation precision with the maximum simulation error of 7.42% is higher for model IV than model III. The simulation precision of the loss factor at different ambient temperatures is higher for model III (simulation error 1.30%-3.91%) than model IV (simulation error 2.31%-9.55%).

4. Three-dimensional restoring force for viscoelastic dampers

Equivalent stiffness and equivalent damping model (Chang *et al.* 1993) is the most convenient model for establishing the restore force of VED. Though this model can reflect the dynamic characteristic of VED, it doesn't embody any frequency-temperature dependence characteristic of VED. Therefore, three dimensional restore forces of VED are derived by the combination of equivalent stiffness and equivalent damping model and improved equivalent standard solid model presented in the above section

$$p_{vex} = k'_x x + \frac{\eta_x k'_x}{\omega_x} \dot{x} \quad (11)$$

$$p_{vey} = k'_y y + \frac{\eta_y k'_y}{\omega_y} \dot{y} \quad (12)$$

$$p_{ve\theta} = k'_\theta \theta + \frac{\eta_\theta k'_\theta}{\omega_\theta} \dot{\theta} \quad (13)$$

where p_{vex} , p_{vey} and $p_{ve\theta}$ are X-axis translational restore force, Y-axis translational restore force and Z-axis rotational restore moment, respectively. $k'_x = G_x A / \tau$, $k'_y = G_y A / \tau$ and $k'_\theta = G_\theta I_p / \tau$ are X-axis translational stiffness, Y-axis translational stiffness and Z-axis rotational stiffness, respectively. A and τ are shear area and thickness of viscoelastic material. $G_i = G(\omega_i)$, $i = x, y, \theta$, is the storage modulus and $\eta_i = \eta(\omega_i)$, $i = x, y, \theta$, is the loss factor. The expression of polar moment of inertia is $I_p = \beta h b^3$ for rectangular shape of viscoelastic material layer and is $I_p = \pi d^4 / 32$ for circular shape of viscoelastic material layer, where h , b are the length and width of viscoelastic material layer, β is a coefficient related to the ratio of h to b and d is the diameter of viscoelastic material layer.

5. Parameter research for multi-dimensional seismic response control

The equations of motion for a single storey mass eccentric platform with the new-type VED subjected to multi-component seismic actions are

$$\mathbf{M}_{3 \times 3} \ddot{\mathbf{U}}_{3 \times 1} + \mathbf{C}_{3 \times 3} \dot{\mathbf{U}}_{3 \times 1} + \mathbf{K}_{3 \times 3} \mathbf{U}_{3 \times 1} + \mathbf{P}_{VE 3 \times 1} = -\mathbf{M}_{3 \times 3} \ddot{\mathbf{U}}_{g 3 \times 1} \quad (14)$$

where

$$\mathbf{M}_{3 \times 3} = \begin{bmatrix} m & 0 & -m e_y \\ 0 & m & m e_x \\ -m e_y & m e_x & J_R \end{bmatrix}, \quad \mathbf{K}_{3 \times 3} = \begin{bmatrix} k_x & 0 & 0 \\ 0 & k_y & 0 \\ 0 & 0 & k_\theta \end{bmatrix}, \quad \mathbf{P}_{VE 3 \times 1} = \begin{bmatrix} p_{vex}(\dot{x}, x) \\ p_{vey}(\dot{y}, y) \\ p_{ve\theta}(\dot{\theta}, \theta) \end{bmatrix}, \quad \ddot{\mathbf{U}}_{g 3 \times 1} = \begin{Bmatrix} \ddot{u}_g \\ \ddot{v}_g \\ \ddot{\phi}_{gz} \end{Bmatrix},$$

$$\mathbf{U}_{3 \times 1} = \begin{Bmatrix} x \\ y \\ \theta \end{Bmatrix}, \quad \dot{\mathbf{U}}_{3 \times 1} = \begin{Bmatrix} \dot{x} \\ \dot{y} \\ \dot{\theta} \end{Bmatrix} \quad \text{and} \quad \ddot{\mathbf{U}}_{3 \times 1} = \begin{Bmatrix} \ddot{x} \\ \ddot{y} \\ \ddot{\theta} \end{Bmatrix} \quad \text{are mass matrix, stiffness matrix, restore force vector,}$$

earthquake acceleration vector, displacement response, velocity response and acceleration response of the platform. e_x and e_y are eccentricity along X-axis and Y-axis. J_R is moment of inertia of platform. The damping matrix in the equation is assumed as Rayleigh damping

$$\mathbf{C}_{3 \times 3} = \alpha \times \mathbf{M}_{3 \times 3} + \beta \times \mathbf{K}_{3 \times 3} \quad (15)$$

And then the equations of motion for a multi-storey mass eccentric platform with the new-type VED subjected to multi-component seismic actions are

$$\mathbf{M}_{3n \times 3n} \ddot{\mathbf{U}}_{3n \times 1} + \mathbf{C}_{3n \times 3n} \dot{\mathbf{U}}_{3n \times 1} + \mathbf{K}_{3n \times 3n} \mathbf{U}_{3n \times 1} + \mathbf{P}_{VE3n \times 1} = -\mathbf{M}_{3n \times 3n} \mathbf{E}_{3n \times 3} \ddot{\mathbf{U}}_{g3 \times 1} \quad (16)$$

It is noted that the elements in restore force vector $\mathbf{P}_{VE3n \times 1}$ are functions of story drift and story velocity, while other matrices are similar to the corresponding term in Eq. (14). $\mathbf{E}_{3n \times 3}$ is the influence coefficient matrix with the expression

$$\mathbf{E}_{3n \times 3} = \begin{bmatrix} 1 & 0 & 0 & \cdots & 1 & 0 & 0 \\ 0 & 1 & 0 & \cdots & 0 & 1 & 0 \\ 0 & 0 & 1 & \cdots & 0 & 0 & 1 \end{bmatrix}^T \quad (17)$$

Based on typical Penzien model (Bi 1989), three platform systems with seven floors are selected in numerical calculation representing short-period, medium-period and long-period platform systems. The first three natural frequencies of the platforms are listed in Table 5. The dimension of platform deck is 44 m×16 m with dead load of 76010.8 kN and live load of 12000 kN. The eccentricity of platform is assumed by the distribution of live load on deck, and two special cases in Fig. 7 are considered in this paper. The typical earthquake acceleration records selected in Table 6 represent four types of ground soil. Randomness of earthquake input direction is considered in analysis and bidirectional acceleration input is used in this paper.

Table 5 The first three natural frequencies for different platforms

Frequency/Hz	Short-period	Medium-period	Long-period
f_1 (translational)	0.6744	0.4621	0.1666
f_1 (translational)	0.9105	0.6239	0.2249
f_3 (rotational)	1.0122	0.6936	0.2501

Table 6 Typical earthquake motions representing four types of ground condition

Typical earthquake records	Type I	Type II	Type III	Type IV
Earthquake name	Michoacan Mexico (1985)	Imperial Valley (1979)	Kern County (1952)	Tangshan (1976)
Station name	La Union	El Centro, Array #10	Taft	Tianjin Hospital
Peak value of acceleration	n00e: 1.6279 n90e: 1.4706	n21e: 2.2169 n69w: 1.6821	n21e: 1.5270 n69e: 1.7590	NS: 1.4580 EW: 1.0418

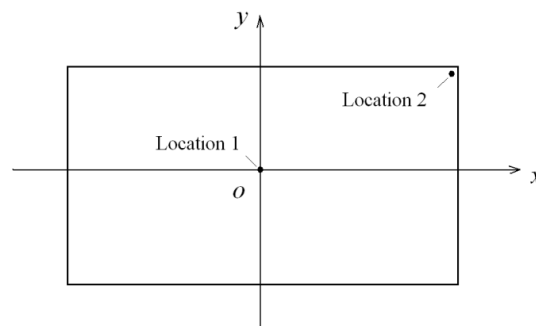


Fig. 7 Graphical diagram for the locations of live load

5.1 Size dimension effect of Viscoelastic material

In this section, rectangular layer shape of viscoelastic material with 2.5 the ratio of length to width, 10 mm thickness is assumed and medium-period eccentric platform with totally seven VEDs installed in the geometry center of each storey is chosen for numerical calculation. Seven VEDs installed in the geometry center of each storey are selected to lower the impact of non-uniform distribution of VEDs on the platform system. Ambient temperature is 20 °C. The translational stiffness ratio of VED to the bottom floor of platform is chosen from 5% to 50% to weigh the size dimension effect of viscoelastic material. The relation curves between maximum storey drift, maximum storey rotation, maximum acceleration on deck and the stiffness ratio are shown in Fig. 8 to Fig. 10.

It is shown from the results that the maximum storey drift and the maximum acceleration on deck can be distinctly decreased with the increase of the stiffness ratio for four types of ground while the influence of size dimension effect on the control effect of the maximum storey rotation is associated with the ground type. For La Union and Taft earthquake, the larger the stiffness ratio is the better the control effect will be. For El Centro and Tianjin earthquake, the maximum storey rotation will increases at first then decreases with the increase of the stiffness ratio.

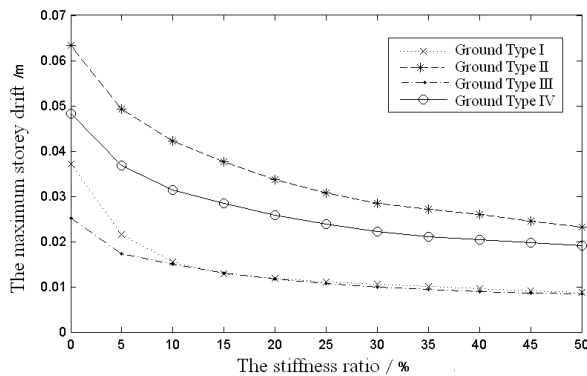


Fig. 8 The relationship curves between maximum story drift and stiffness ratio

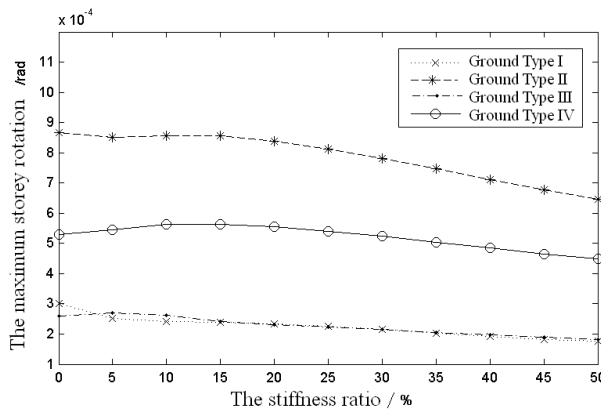


Fig. 9 The relationship curves between maximum story rotation and stiffness ratio

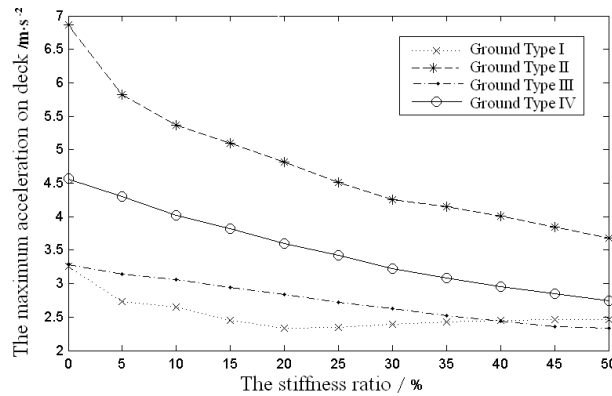


Fig. 10 The relationship curves between maximum acceleration of top floor and stiffness ratio

5.2 Shape effect of Viscoelastic material

The expression of polar moment of inertia is dependent on the material shape of VED. Six kinds of shapes are selected to analyze the influence of shape effect on the rotational response control on the premise of identical shear area. Shape 1-Shape 2 are rectangular sections with the length-width ratio are 2.5 and 1.0, respectively. Shape 3 is circular section. Shape 4, Shape 5 and Shape 6 are ring sections with the inner-outer diameter ratio are 0.3, 0.5 and 0.7. The related parameters used in the calculation are coincident with Section 5.1 unless otherwise stated. The increment of decreasing amplitude ratio on rotational response is defined as the difference of decreasing amplitude ratio between each shape and Shape 1. Fig. 11 gives the relationship curves of this increment with different stiffness ratio, different period platforms and different ground types, respectively.

Numerical results show that the control effect of maximum rotational response is related to the viscoelastic material shape. The order of better control effect is Shape 6, Shape 5, Shape 4, Shape 3, Shape 2 and Shape 1. The difference of decreasing amplitude ratio caused by different shapes is also related to the stiffness ratio, the period of platform and the ground type. However, it is also noted from the numerical results that the maximum difference of decreasing amplitude ratio caused by different shapes is only 0.4%. This phenomena reveals that the energy dissipation capacity is very limited only by the single torsional deformation of VED. In practical engineering application, translational deformation of VED should be fully used to dissipate much shake energy.

5.3 Ambient temperature effect

In this section 30 kinds of cases are calculated with different ambient temperatures from 1 °C to 30 °C for symmetric platform with live load located in Location 1. The translational stiffness ratio of VED to the bottom floor of platform is assumed to be 20%. Other related parameters used in the calculation are coincident with Section 5.1.

The maximum storey drift and the maximum deck acceleration for the uncontrolled platform system are listed in Table 7. Fig. 12 gives the relationship curves between the maximum absorption ratios of storey drift and deck acceleration and ambient temperatures. The maximum

absorption ratio of storey drift JZV_{xy} and the maximum absorption ratio of deck acceleration JZV_a are defined as follows

$$JZV_{xy} = \frac{(xy_{\text{withoutVED}}) - (xy_{\text{withVED}})}{xy_{\text{withoutVED}}} \times 100\% \tag{18}$$

$$JZV_a = \frac{(a_{\text{withoutVED}}) - (a_{\text{withVED}})}{a_{\text{withoutVED}}} \times 100\% \tag{19}$$

where $xy_{\text{withoutVED}}$ and $a_{\text{withoutVED}}$ are the maximum storey drift and the maximum deck acceleration in two horizontal directions for the uncontrolled platform system. The parameters xy_{withVED} and a_{withVED} are the maximum storey drift and the maximum deck acceleration in two horizontal directions for the platform installed with VEDs.

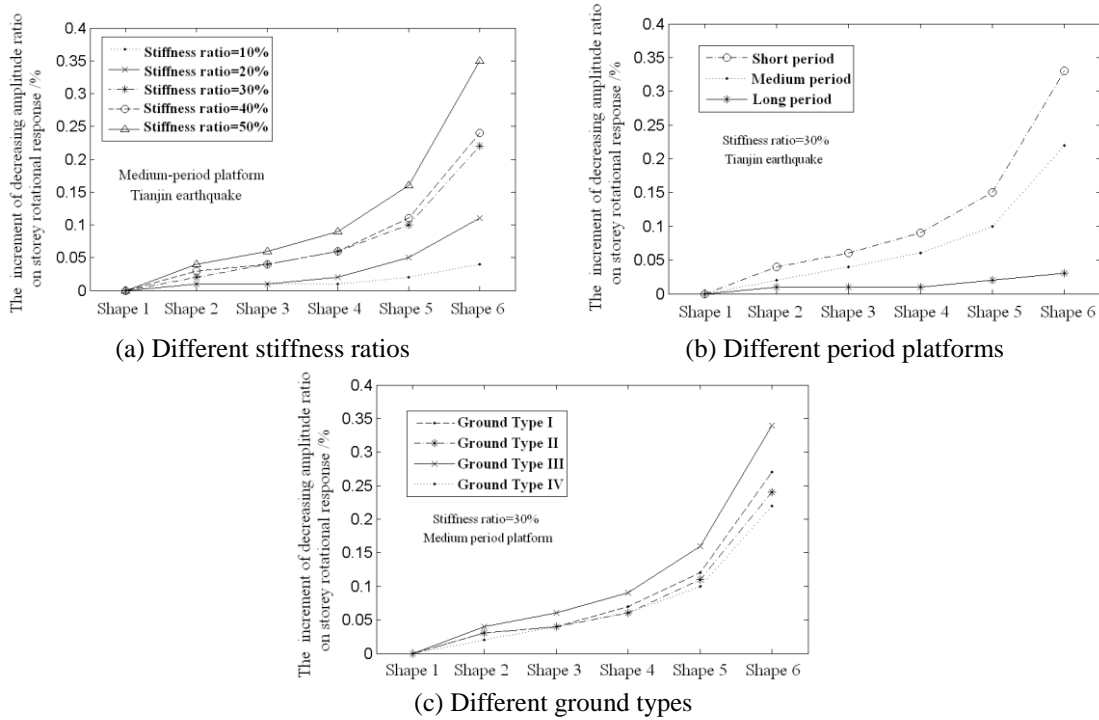


Fig. 11 The increment of absorption ratio on story rotation due to different shapes

Table 7 The maximum story drift and top floor acceleration for the four types of ground motion

Earthquake station name	Maximum storey drift/m	Maximum deck acceleration/m·s ⁻²
La Union	0.0374	3.2912
El Centro	0.0645	6.9047
Taft	0.0259	3.3077
Tianjin	0.0374	3.2912

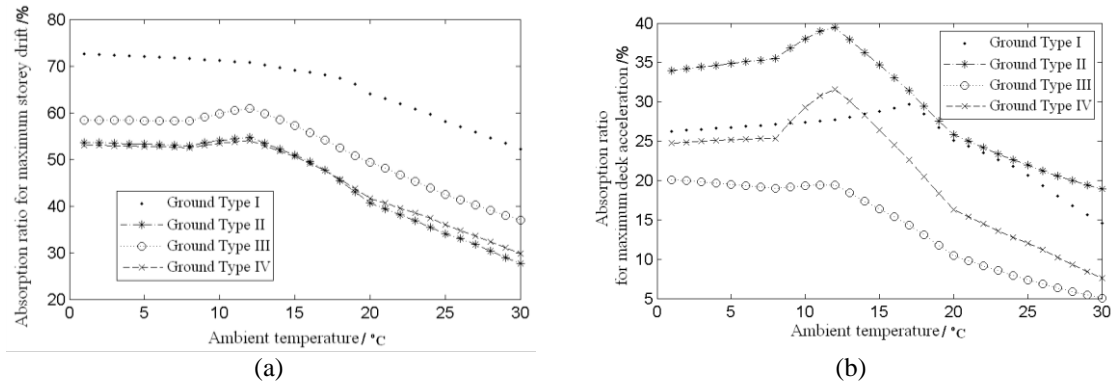


Fig. 12 The relationship curves between absorption ratio and temperature

Numerical results show that the relationship curves of absorption ratio and ambient temperature for storey drift and deck acceleration have similar rules. The control effect is almost the same when ambient temperature is below 12°C and then it will get worse with the increasing of ambient temperature that is higher than 12°C . The optimal control effect is obtained when ambient temperature is just near 12°C . This phenomenon is essentially caused by the temperature dependency property of storage modulus and loss factor.

5.4 Response frequency effect of viscoelastic dampers

In this section, the stiffness ratio is taken as 30% and three platform systems with different periods are calculated for the four types of ground conditions. Other related parameters used in the calculation are coincident with Section 5.1. Typical dynamic response results are listed in Table 8. Fig. 13 gives the time-history curves of the maximum storey drift for the three platform systems.

It is shown from Table 8 that VED has a great effect on reducing dynamic response of platforms (especially for storey drift) and this effect do have relations with the frequency-dependence property of VED. Two factors including the natural period of platform and the frequency characteristic of earthquake motion can influence the response frequency effect of viscoelastic dampers. It must be noted that the rotational response and the deck acceleration may be amplified in some cases when VEDs are installed in the long-period platform. For the long-period platform, the stiffness of the uncontrolled platform is comparatively small. The viscoelastic dampers installed in platform have two aspects of impact on the earthquake response: increasing the stiffness and increasing the damping. Therefore the impact of increasing the stiffness and the impact of increasing the damping are very close for the long-period platform. In addition, it is indicated from Fig. 13 that the maximum storey drift for different uncontrolled platform systems is usually present to the top floor or upper floor in four types of ground condition, while for the controlled platform systems with VEDs it is often present to the bottom floor or lower floor. The critical incidence of ground motion may be different for the platform systems with and without VED installed, such as the medium-period platform in Ground Type III and the long-period platform in Ground Type II. Therefore, it is necessary to consider the randomness of earthquake input direction in order to obtain the reliable results.

6. Conclusions

Analytical studies on the restoring force model of VED under various ambient temperatures and frequency-dependence excitations and the seismic behavior of platform systems subjected to different earthquake ground motions representing four types of ground condition have been carried out. The effect of size dimension and shape effect of viscoelastic material on the seismic response control is also studied. Two improved models of improved equivalent standard solid model and improved fractional derivative model can obtain high simulation precision and is suitable to be used in numerical calculation. The analytical results show that the new type viscoelastic damper is capable of mitigating the multi-dimensional seismic response of offshore platform. The response control effect of VED is more dependent on the response frequency effect and ambient temperature though it can be optimized by the proper design of the size and shape of VED.

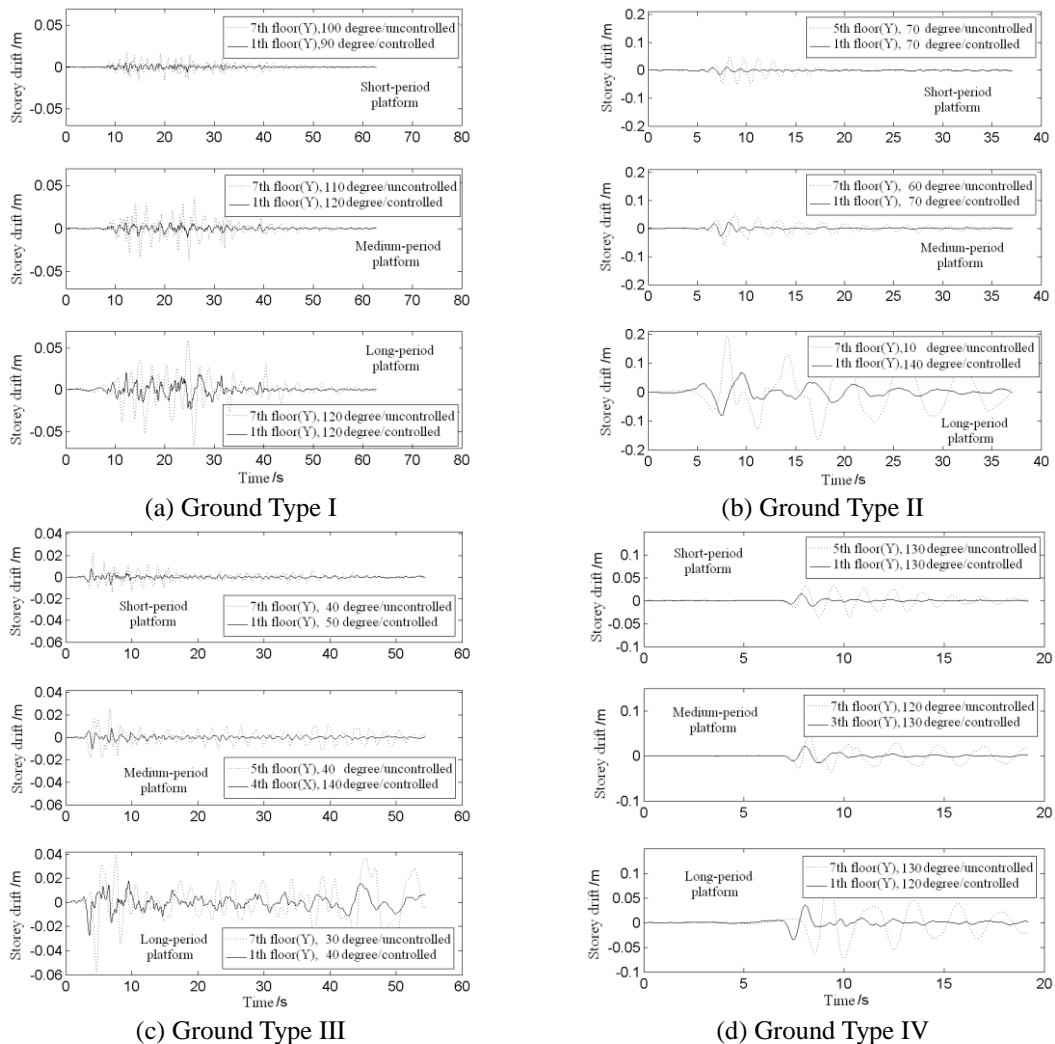


Fig. 13 The time history curves of story drift before and after the installation of VED dampers

Table 8 The maximum response and the absorption ratio for four ground conditions and three platforms

Platform	Ground Type	Maximum storey drift/m			Maximum storey rotation/ 10^{-4} rad			Maximum deck acceleration/ $m\cdot s^{-2}$		
		Uncontrolled	Controlled	JZV /%	Uncontrolled	Controlled	JZV /%	Uncontrolled	Controlled	JZV /%
Short period	I	0.0178	0.0069	61.41	2.5749	1.6644	35.36	4.2444	2.8721	32.33
	II	0.0514	0.0157	69.46	4.4979	2.6435	41.23	7.1324	3.0438	57.32
	III	0.0213	0.0076	64.55	1.9546	1.5205	22.21	3.6512	3.0758	15.76
	IV	0.0354	0.0148	58.06	4.7213	3.5526	24.75	5.9789	2.9576	50.53
Medium period	I	0.0372	0.0107	71.29	3.1441	2.0810	33.81	3.2524	2.4100	25.90
	II	0.0633	0.0275	56.53	9.0429	7.4950	17.12	6.8562	4.3816	36.09
	III	0.0251	0.0101	59.73	2.7122	2.0283	25.22	3.2884	2.5906	21.22
	IV	0.0483	0.0214	55.74	5.5304	5.0050	9.50	4.5650	3.4720	23.94
Long period	I	0.0678	0.0231	65.89	4.9921	5.4185	-8.54	2.0828	1.9641	5.70
	II	0.1941	0.0810	58.30	24.970	19.095	23.53	3.6288	3.4769	4.19
	III	0.0579	0.0272	52.96	7.1775	4.7068	34.42	2.1913	2.5486	-16.31
	IV	0.1092	0.0357	67.34	3.5353	2.0438	42.19	1.7609	2.2356	-26.96

References

- Bergman, D.M. and Hanson, R.D. (1993), "Viscoelastic mechanical damping devices tested at real earthquake displacements", *Earthq. Spectra*, **9**(3), 389-417.
- Bi, J.J. (1989), *Offshore Mechanics (in Chinese)*, Shanghai, Tongji University Press.
- Chang, K.C., Lai, M.L., Soong, T.T., Hao, D.S. and Yeh, Y.C. (1993), *Seismic Behavior and Design Guidelines for Steel Frame Structures with Added Viscoelastic Dampers*, NCEER 93-0009, National Center for Earthquake Engineering Research, Buffalo, NY.
- Chang, K.C., Soong, T.T., Oh, S.T. and Lai, M.L. (1992), "Ambient temperature on a viscoelastically damped structure", *J. Struct. Eng. - ASCE*, **118**(7), 1955-1973.
- Chang, K.C., Soong, T.T., Oh, S.T. and Lai, M.L. (1995), "Seismic behavior of steel frame with added viscoelastic dampers", *J. Struct. Eng. - ASCE*, **121**(10), 1418-1426.
- Inaudi, J.A. (1996), "Time-domain analysis of linear hysteretic damping", *Earthq. Eng. Struct. D.*, **25**, 529-545.
- Kasai, K., Munshi, J.A., Lai, M.L. and Maison, B.F. (1993), "Viscoelastic damper hysteretic model: theory, experiment and application", *Proceeding of the ATC-17-1 Seminar on Seismic-Isolation, Passive Energy Dissipation and Active Control*, Redwood City, CA: 521-532.
- Lee, H.H. (1997), "Stochastic analysis for offshore structures with added mechanical dampers", *Ocean Eng.*, **24**(9), 817-834.
- Lin, R.C., Liang, Z., Soong, T.T. and Zhang, R.H. (1991), "An experimental study on seismic behavior of viscoelastically damped structures", *Eng. Struct.*, **13**(1), 75-84.
- Ma, H.L. and Lu, J.H. *et al.* (2004), "Viscoelastic damper vibration control of platform with pole assignment technique(in Chinese)", *J. Ship Mech.*, **8**(4), 116-120.
- Mahmoodi, P. (1969), "Structural dampers", *J. Struct. Eng. Div. - ASCE*, **95**(10), 1661-1672.
- Ou, J.P. and Xu, L. *et al.* (2002), "Damping isolation system and its vibration-suppressed effectiveness analysis for offshore platform jacket structures (in Chinese)", *Earthq. Eng. Eng. Vib.*, **22**(3), 115-122.
- Ou, J.P., Duan, Z.D., Xiao, Y., Wei, J., Li, T. and Sun, B. (1999), "Ice-induced vibration analysis of JZ20-2MUQ offshore platform using in-situ ice force histories (in Chinese)", *Ocean Eng.*, **17**(2), 70-78.
- Ou, J.P., Xiao, Y.Q., Duan, Z.D., Zou, X.Y., Wu, B. and Wei, J.S. (2000), "Ice-induced vibration control of

- JZ20-2MUQ platform structure with viscoelastic energy dissipators (in Chinese)", *Ocean Eng.*, **18**(3), 9-14.
- Sui, J.Y. (2002), *Experimental study and engineering application of viscoelastic damper and energy dissipation brace (in Chinese)*, Ph.D. Dissertation, Southeast University, Nanjing.
- Wu, B. and Guo, A.X. (1998), "Study on properties of viscoelastic dampers (in Chinese)", *Earthq. Eng. Eng. Vib.*, **18**(2), 108-116.
- Xu, Z.D. (2001), *Experimental study on the (lead) viscoelastic structure*, Ph.D. Dissertation (in Chinese), Xi'an Architecture & Technology University, Xi'an.
- Xu, Z.D. (2007), "Earthquake mitigation study on viscoelastic dampers for reinforced concrete structures", *J. Vib. Control*, **13**(1), 29-43.
- Xu, Z.D. and Zhao, H.T. *et al.* (2001), "Equivalent standard solid model of the viscoelastic damper (in Chinese)", *Build. Struct.*, **31**(3), 67-69.
- Zhou, Y. (2006), *Damping structural design by viscoelastic damper (in Chinese)*, Wuhan University of Technology Press, Wuhan, China.